Structure Development in Melt Spinning Poly(vinylidene Fluoride) Fibers and Tapes

YIMIN WANG,* MUKERREM CAKMAK, and JAMES L. WHITE,
Polymer Engineering Center, University of Akron, Akron, Ohio 44325

Synopsis

A series of poly(vinylidene fluoride)s of varying molecular weight have been melt spun to form fibers and tapes. These have been characterized with wide angle X-ray diffraction (WAXD), differential scanning calorimetry (DSC), birefringence, and small angle light scattering (SALS). WAXD and DSC have detected both the α and β crystal structures in melt spun fibers with the relative amount of β increasing with drawdown stress. WAXD and birefringence have been used to detect orientation in the fibers. Hermans–Stein orientation factors have been computed for the α-phase as a function of drawdown stress. Superstructure has been investigated using SALS. The mechanical properties of fibers have been determined with a tensile testing machine and correlated with orientation and spinline stress.

INTRODUCTION

Poly(vinylidene fluoride) is an important industrial resin finding applications as sheets, tubes, fittings, gears, bearings, and coatings for the chemical industry. Its most celebrated applications are due to is piezo- and pyroelectric behavior.[1,2] There has been little study of its fiber forming characteristics, though it has been melt-spun to form fishing lines. The crystal structure of poly(vinylidene fluoride) has been investigated extensively, associated with the discovery that it is polymorphic.[3–10] Four crystalline forms have been identified. Generally, polymer formed by cooling a quiescent melt forms a pseudohelical structure (TG^+TG^-)[4,6–8] known as the α form (or form II). Cold drawing of isotropic α films produces a crystal structure containing zigzag chains (β form).[3,7,8] Other forms may be produced by applied electrical fields.

In the present paper, we will present an experimental study of structure development in melt spinning of fibers and tapes of poly(vinylidene fluoride). The influence of processing conditions on the crystalline forms developed and their orientation is determined as a function of spinning conditions and molecular weight. The general viewpoint of this paper is similar to that developed in earlier papers by one of us.[11,12]

BACKGROUND

Crystal Structure

The four crystalline structures developed in polyvinylidene fluoride (PVF_2) have been summarized in Table I. The α and β structure (forms II

* Permanent address: East China Institute of Textile Science and Technology, Shanghai, China.

Journal of Applied Polymer Science, Vol. 30, 2615–2632 (1985)
 CCC 0021-8995/85/062615-18$04.00

TABLE I
Crystalline Forms of Poly(vinylidene Fluoride)

Crystalline form	Chain conformation	Unit cell type	Unit cell dimensions (Å)	References
α, form II	TG^+TG^-	Monoclinic	$a = 4.96$, $b = 9.64$, $c = 4.62$, $\beta = 90°$	4, 6–8
β, form I	TTTTT	Orthorhombic	$a = 8.58$, $b = 4.91$, $c = 2.56$	3, 7, 8
γ, form III	$TTTG^+TTTG^-$	Orthorhombic	$a = 4.97$, $b = 9.66$, $c = 9.18$	10
δ, form IV (polar α)	TG^+TG^-	Orthorhombic	$a = 4.96$, $b = 9.64$, $c = 4.62$	9

and I) are those primarily of concern here as they are developed by mechanical forms. The α form which has alternating *trans* and *gauche* conformations (TG^+TG^- TG^+) is formed by direct cooling from the quiescent melt. The β form, which is a zigzag alternating *trans* structure (TTTTTT), is formed by low temperature drawing of the α.

The primary manner of determining the crystalline forms of PVF_2 is wide angle X-ray diffraction (WAXD). The major reflections of these forms are summarized in Table II. The characteristic distances d_{hkl} of the principal Bragg reflection peaks differ, making the phases clearly distinguishable. The intensities of the peaks can be used to distinguish the relative amounts of the two phases present.

Orientation

We are concerned with the orientation of the polymer chains and the crystallographic axes relative to the fiber axis. Most generally, this can be

TABLE II
Principal X-Ray Reflections of Polyvinylidene Fluoride

Form	Miller's indices of reflecting plane	Interplanar spacing (Å)
α	110	4.45
	020	4.82
	200	2.98
	010	5.096
β	200	4.27
	110	
	310	2.46
	020	
	510	1.61
	420	
	130	
	400	2.12
	220	
	201	2.19
	111	

expressed in orientation distribution functions of the type described by Muller[13] and Roe and Krigbaum.[14] We shall in this paper represent chain orientation in terms of the Hermans orientation factor[15,16]

$$f_c = \frac{3\,\overline{\cos^2 \phi_{cl}} - 1}{2} \tag{1}$$

where ϕ_{cl} represents the angle between the chain axis and the fiber axis. More generally, following Stein,[17] we shall represent orientation of crystallographic axes in terms of the Hermans–Stein orientation factors defined by

$$f_j = \frac{3\,\overline{\cos^2 \phi_j} - 1}{2} \tag{2}$$

where j represents the crystallographic axis.

Experimentally one determines the f_j orientation factors from wide angle X-ray diffraction as described by Stein[17] in his original paper which treats polyethylene. This has been applied by various investigators to other polymer systems.[11,12] There seems, however, to be no previous computations of uniaxial orientation in PVF_2.

For the α form, the (110), (200), and (020) reflections may be used to compute f_a and f_b. The (200) and (020) may be used directly to give the orientation factor. The (110) may be used in conjunction with the (200) in the manner described by Stein[17] to compute the orientation factors f_a and f_b from the (110) and (200) planes. We may show that

$$\overline{\cos^2 \phi_{c,z}} = 1 - 1.2647\,\overline{\cos^2 \phi_{110}} - 0.7353\,\overline{\cos^2 \phi_{200}} \tag{3}$$

The f_c orientation factor may also be computed from the orthogonality of the unit cell through the relation

$$f_c = -(f_a + f_b) \tag{4}$$

EXPERIMENTAL

Materials

The polymers used in this study are commercially available grades produced by Solvay and Pennwalt. They are summarized in Table III. The polymers primarily differ from each other in molecular weight.

Formation of Fibers and Tapes

Fibers were melt-spun from an Instron capillary rheometer using a capillary die of diameter 0.12 mm and length/diameter ratio of 39. A melt temperature of 220°C was used. The fibers were taken up at varying drawdown ratios V_L/V_0 from 20 to 747. The fibers were spun through air, and tensions were measured during melt spinning using a Rothschild Tensometer.

TABLE III
Materials Used in This Study

Our designation	Supplier	Commercial name	Approximate apparent shear viscosity (220°C and 100 s^{-1}) (Pa · s)
		PVDF SOLEF	
PVF_2-1		1012	3000
2	Solvay and Cie	1010	1700
3		1008	800
4		1006	—
5	Pennwalt Corp.	KYNAR 901	2200

Tapes were extruded from an Instron capillary rheometer using a die of diameter 0.0381 cm and length 0.635 cm at 220°C. Drawdown ratios V_L/V_0 were in the range of 12–85.

X-Ray Diffraction

The fibers produced by melt spinning were examined with an X-ray diffractometer. Flat-plate X-ray camera photos were taken with CuK_α radiation, with the sample-to-film distance of 35 mm and with the X-ray beam perpendicular to the fiber axis or film surface. Generally speaking, a flat-plate photo is sufficient to determine which phase is present.

Crystalline orientation was interpreted quantitatively using diffractometer scans. Hermans–Stein orientation factors defined by eq. (2) were computed for the α phase using the (110) and (200) reflections. In particular, the chain axis orientation factor was computed using eq. (3).

Birefringence

Birefringence of melt-spun fibers were obtained from optical retardations determined using a Leitz Laborlux-12 polarizing light microscope with a 30 order Berek Compensator.

Differential Scanning Calorimetry

Scans of samples were made using a DuPont Model 1090 Differential Thermal Analyzer. A heating rate of 10°C/min was used. On selected samples which show multiple endotherms, various heating rates were used to study the effect of heating rate on DSC spectra.

Small Angle Light Scattering

The tapes were investigated using a small angle laser light scattering apparatus in our laboratory. The apparatus contains a laser, polarizer, sample holder, and analyzer. H_v patterns were recorded on photographic film.

Mechanical Properties

Uniaxial stress–strain measurements were made on fibers using a Monsanto Tensometer 500. A constant crosshead speed of 2 cm/min were used.

The gauge length was 30 mm. All measurements were carried out at room temperature.

MELT SPINNING AND STRUCTURAL STUDIES

Results

We plot spinline stress as function of drawdown ratio in Figure 1 for the samples studied. The stresses increase monotonically with V_L/V_0 and order among the samples as

$$PVF_2\text{-}1 > PVF_2\text{-}5 > PVF_2\text{-}2 > PVF_2\text{-}3 > PVF_2\text{-}4$$

Wide angle X-ray diffraction patterns for the PVF_2 fibers are shown in Figure 2. It is clear from the diffraction patterns that the filaments are oriented. Typical diffractometer scans are shown in Figure 3. The film patterns exhibit other qualitative variations. New diffraction peaks arise as the drawdown ratio increases, suggesting the formation of a second crystalline phase.

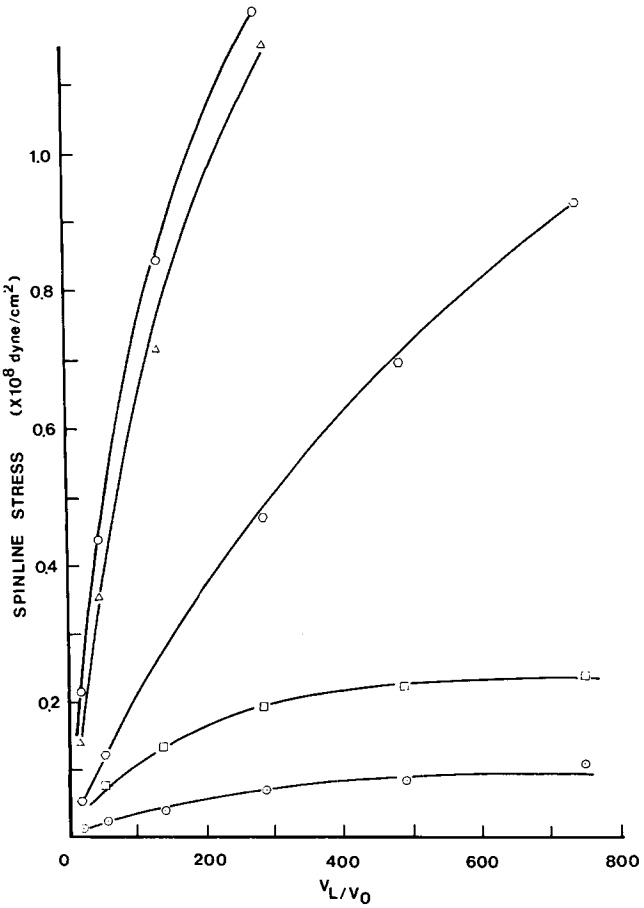

Fig. 1. Spinline stress as a function of drawdown ratio for PVF_2 fibers: (○) PVF_2-1; (⊂) PVF_2-2; (□) PVF_2-3; (⊙) PVF_2-4; (△) PVF_2-5.

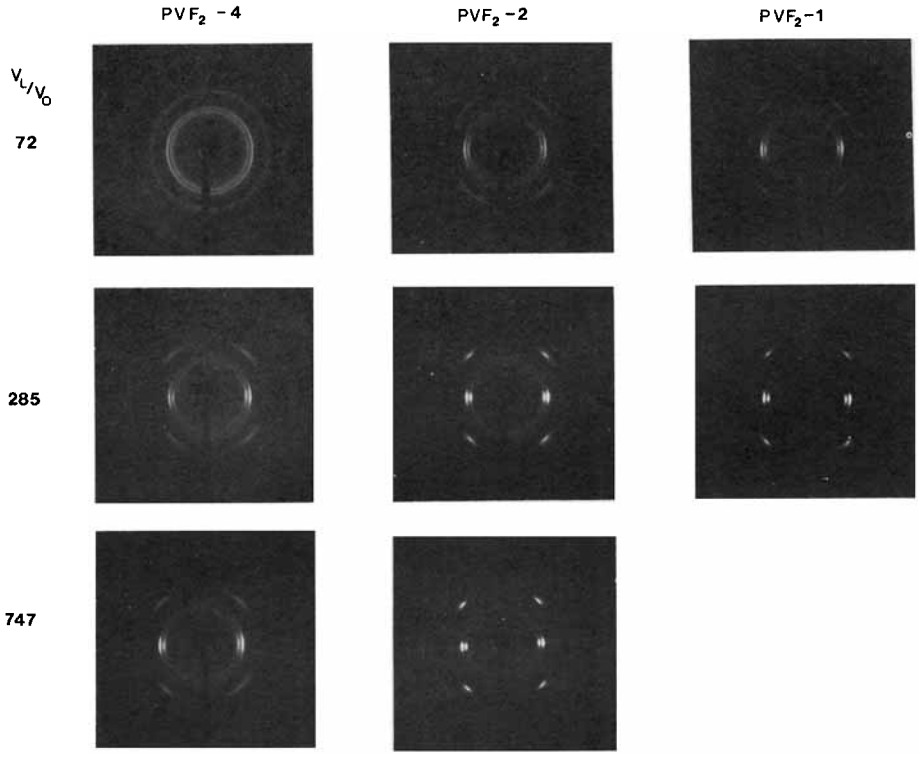

Fig. 2. WAXS patterns of melt spun PVF_2 fibers.

The birefringence of the melt spun fibers is plotted in Figure 4 as a function of V_L/V_0. The birefringence increases in a monotonic manner and order as

$$PVF_2\text{-}1 > PVF_2\text{-}5 > PVF_2\text{-}2 > PVF_2\text{-}3 > PVF_2\text{-}4$$

DSC traces with a scan rate of 10°C/min for the melt-spun fibers are shown in Figures 5(a)–(c). Multiple melting peaks are found. The lower temperature peak is most prevalant in PVF_2-4 at low drawdowns and the higher temperature peak for PVF_2-1 and PVF_2-2 at high drawdown ratios. Essentially identical results are obtained at other scan rates [Fig. 5(d)].

SALS patterns of melt spun tapes are shown in Figure 6. Four-lobed H_v patterns with intensity maxima in the lobes are observed, at low V_L/V_0 for all the samples except PVF_2-1. This sample shows a maximum intensity in the center which decreases with scattering angle. A transition from the four-lobe pattern to the central intensity maximum is found in the other samples as well except sample 4, which continues to show four-lobed patterns at a much higher V_L/V_0 than samples 1, 2, and 5. The V_L/V_0 at which these occur order (from high to low) as

$$PVF_2\text{-}4 > PVF_2\text{-}3 > PVF_2\text{-}2 > PVF_2\text{-}5 > PVF_2\text{-}1$$

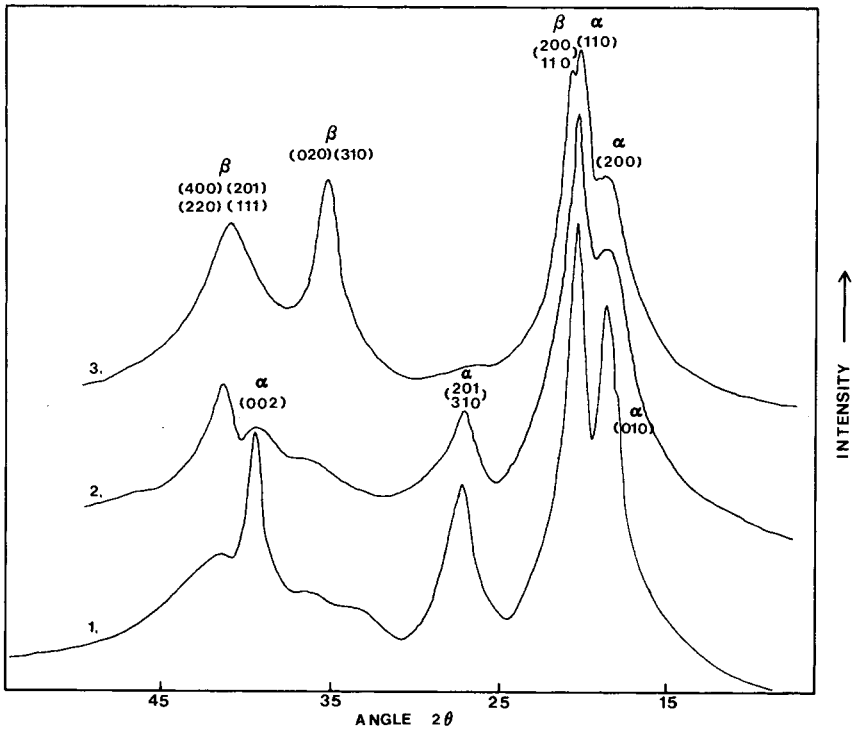

Fig. 3. Wide angle X-Ray diffractometer scans for melt-spun PVF_2 fibers. Samples were mechanically randomized. (1) PVF_2-4; $V_L/V_0 = 285$; (2) PVF_2-1, $V_L/V_0 = 285$; (3) PVF_2-4, cold drawn.

Polymorphism

The WAXS patterns and diffractometer scans (Figs. 2 and 3) give evidence of the existence of both α and β crystalline phases. This view is supported by the DSC traces. The fibers spun at the lowest V_L/V_0 seem to be entirely in the α form. The β form is found in filaments of PVF_2-1, PVF_2-2, and PVF_2-5 produced at higher drawdowns. It is first apparent in PVF_2-1 and at higher V_L/V_0 in PVF_2-5 and eventually in PVF_2-2. No transitions are observed in samples PVF_2-3 and PVF_2-4 even at quite high drawdown ratios. We have determined the relative quantities of the α and β phases in the spun fibers using differential scanning calorimetric traces. The fractional contents of phases α and β were determined by taking the ratio of the area under the α-phase peak to the area under all the melting peaks. The overlapping of these peaks were resolved by using an LSR computer program. At a DSC heating rate of 10°C/min, it is found that, as V_L/V_0 is increased, the proportion of α phase decreases as shown in Figure 5, and there is an increasing proportion of β phase which at a V_L/V_0 285 exceeds 50.8% by volume for sample 1 and 32.4% for sample 2. However, samples 3 and 4 always show only the α form even when the V_L/V_0 ratio is three times than the transition of samples 1 and 2 to contain the β form.

The results of the above paragraph together with Figure 1 suggest that the β form begins to occur at a critical drawdown stress σ. Comparing the data for the three samples exhibiting the formation of the β phase, this

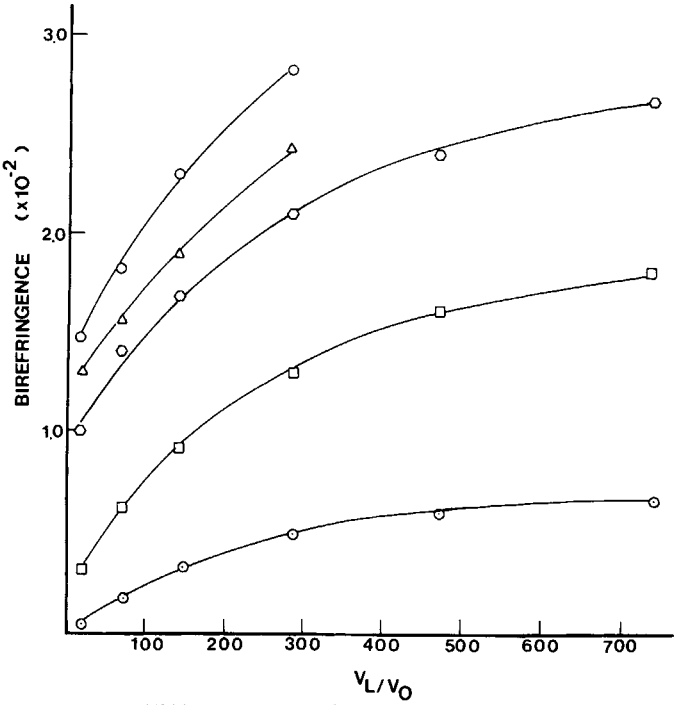

Fig. 4. Birefringence of PVF_2 melt-spun fibers as a function of drawdown ratios: (○) PVF_2-1; (○) PVF_2-2; (□) PVF_2-3; (⊙) PVF_2-4; (△) PVF_2-5.

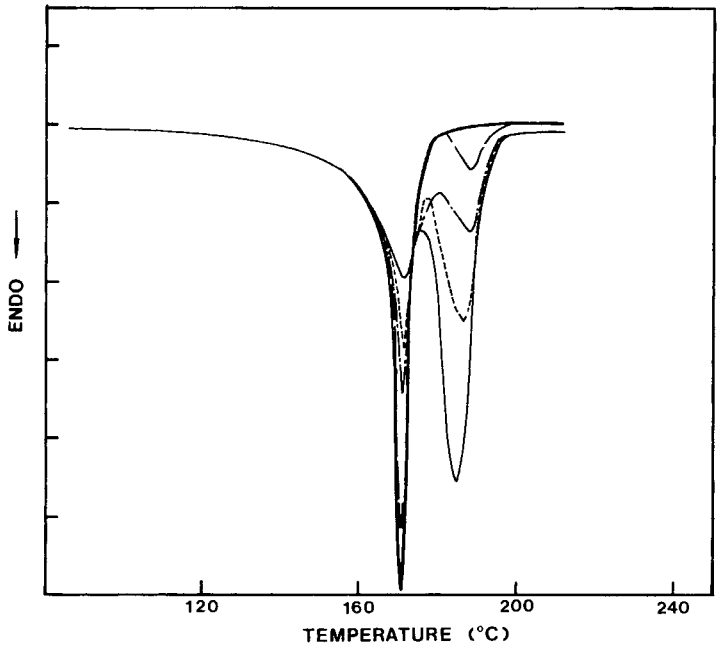

Fig. 5. Differential scanning calorimetry traces of melt PVF_2 spun fibers. (a) Sample 1—PVF_2-1; V_L/V_0: (—) 285; (--) 180; (-·-) 140; (— — —) 70; (—) 40. (b) Sample 2—PVF_2-2; V_L/V_0: (—) 747; (-·-) 285; (— — —) 161. (c) Sample 4—PVF_2-4; V_L/V_0: (—) 747; (—) 474; (-·-) 251; (--) 70. (d) Effect of heating rates (°C/min) on DSC spectra of sample PVF_2-2, $V_L/V_0 = 747$: (1) 5; (2) 20; (3) 40.

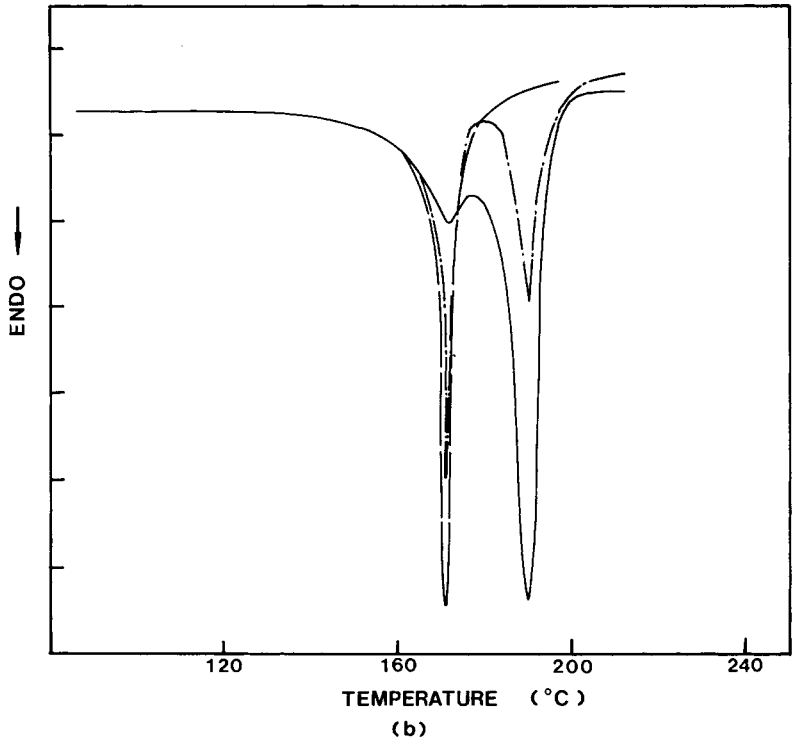

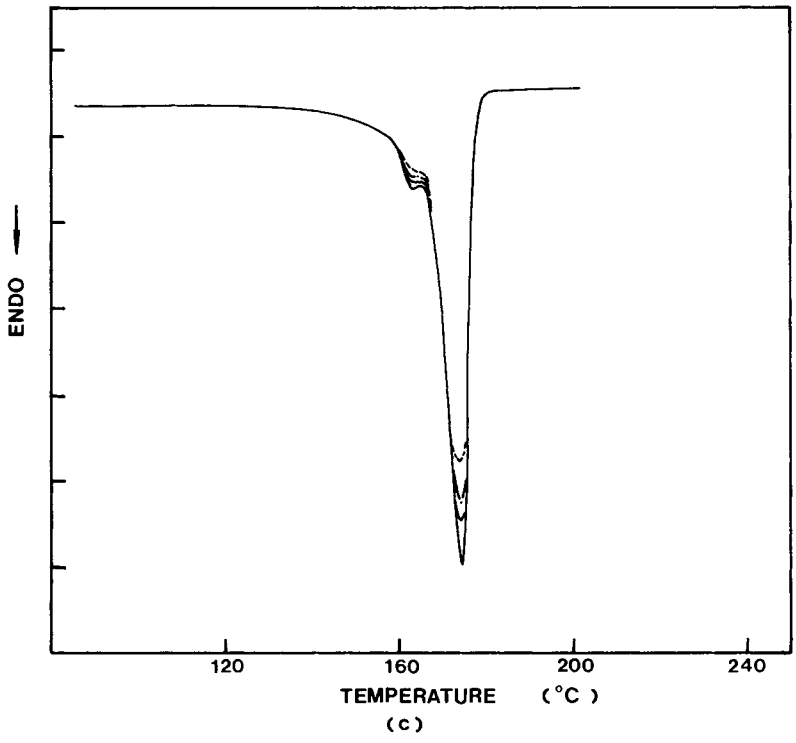

Fig. 5. (*Continued from previous page.*)

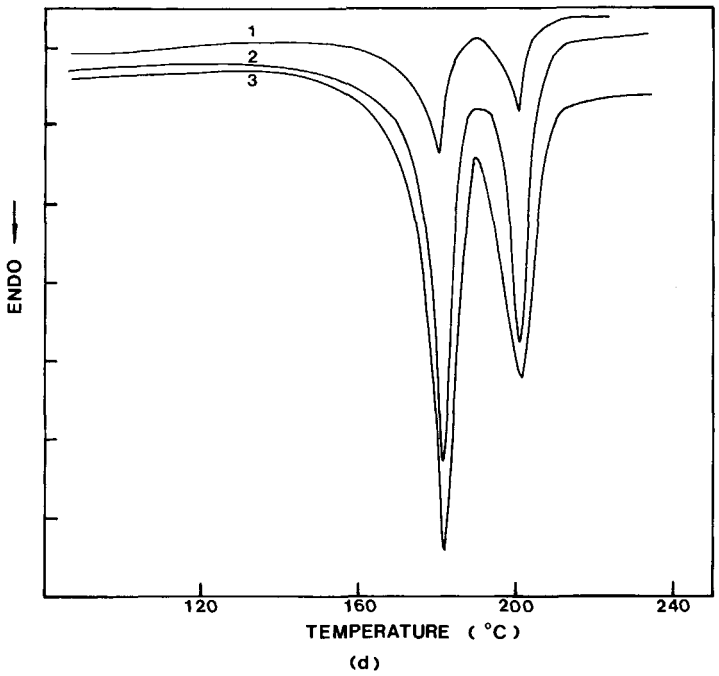

Fig. 5. (*Continued from previous page.*)

seems to arise at a spinline stress of 3×10^6 Pa. The relative quantities of the α and β phases in the spun fiber are plotted as a function of spinline stress in Figure 7.

It would seem to us most likely that the melt is crystallizing to form a mixture of α and β crystals. Orientation of the macromolecules in the melt is determined by the spinline stress.[18] Presumably the β phase starts to form above a specific level of orientation in the melt.

Orientation of Crystallographic Axes in α-Phase

Hermans–Stein orientation factors have been computed from the α phase (110) and (200) reflections. They are plotted as a function of V_L/V_0 in Figure 8. The orientation factors f_c for PVF_2-4 are very small and near zero. It is clear that f_c in the other polymers is positive and a monotonic increasing function of V_L/V_0. f_c orders among the polymers as

$$PVF_2\text{-}1 > PVF_2\text{-}5 > PVF_2\text{-}2 > PVF_2\text{-}3 > PVF_2\text{-}4$$

The f_a and f_b are generally negative with

$$|f_a| > |f_b|$$

and decrease towards -0.5 with increasing drawdown. The magnitude of $|f_a|$ order among the different polymers studied in the same manner as f_c.

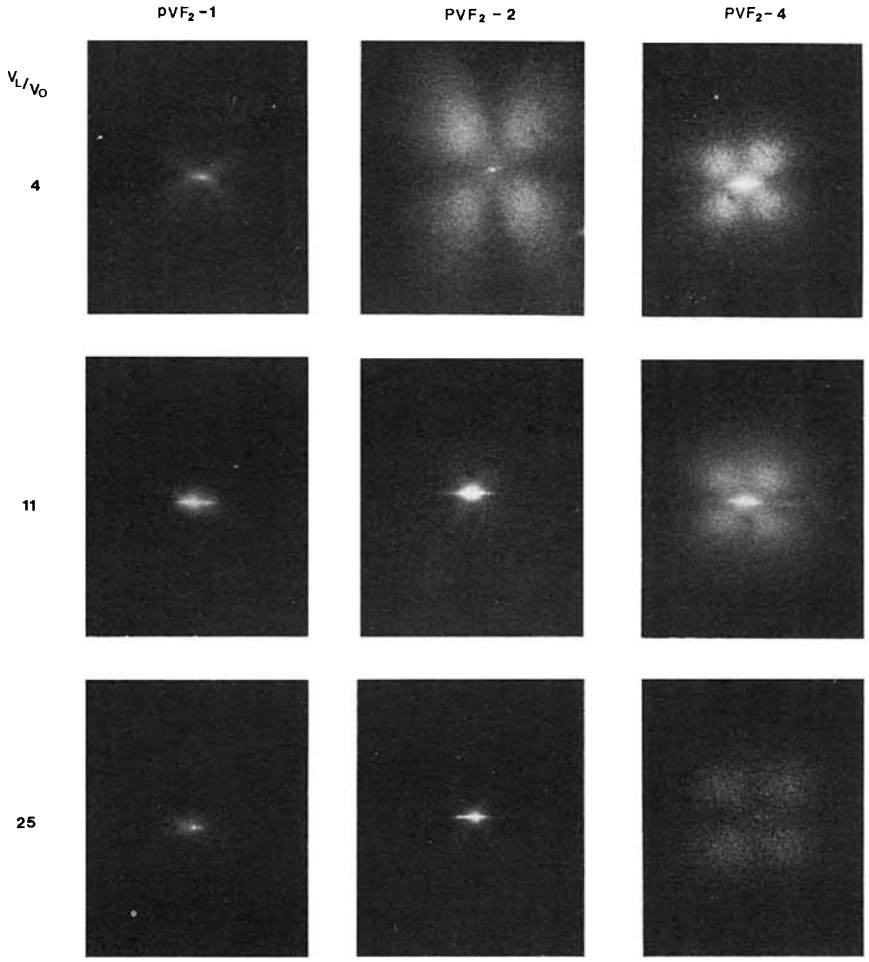

Fig. 6. SALS patterns of melt-spun tapes.

The variations in f_a, f_b, and f_c with spinning conditions described above are similar to those observed with polyolefins[11,19,20] and nylon-6.[12] Nadella et al.[11] showed with different molecular weight polypropylenes that the orientation factors could be correlated uniquely with spinline stress. We make such a plot for our PVF_2 samples in Figure 9. The f_j data correlates with spinline stress.

Birefringence of Fibers

The birefringence of the fibers should, as suggested by Hermans et al.[21] and Stein and Norris,[22] be given by the sums of the birefringence in the different phases and form birefringence. For PVF_2 with two crystalline phases plus an amorphous phase, we have

$$\Delta n = \phi_\alpha f_c^\alpha \Delta_\alpha^0 + \phi_\beta f_c^\beta \Delta_\beta^0 + \phi_{am} f_{am} \Delta_{am}^0 + \Delta n_{form} \quad (5)$$

where Δ_α^0, Δ_β^0, and Δ_{am}^0 are intrinsic birefringence of the α, β, and amorphous

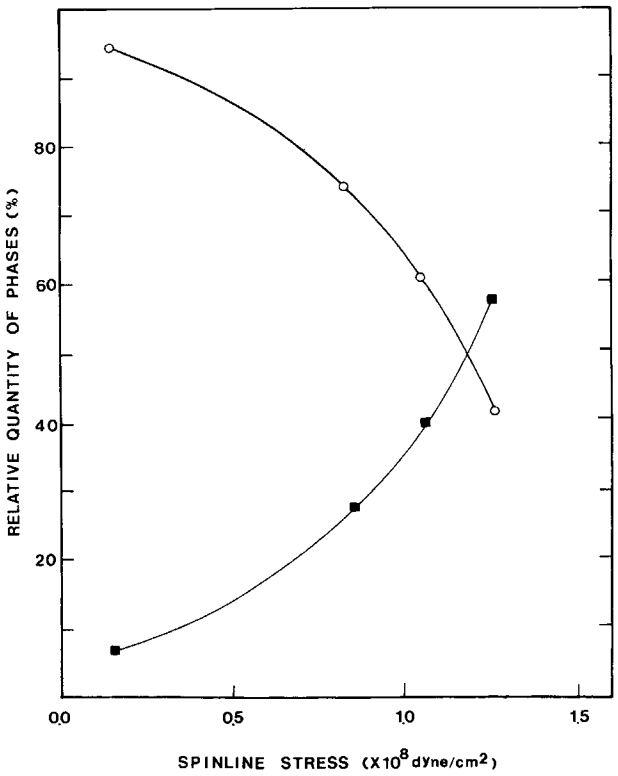

Fig. 7. Relative quantities of α (○) and β (■) phases in PVF_2-1, fibers as a function of spinline stress.

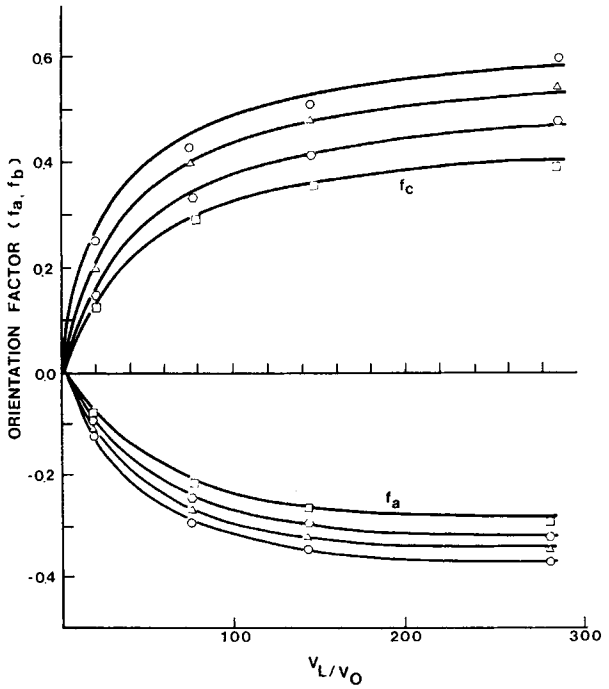

Fig. 8. Hermans–Stein orientation factors as a function of V_L/V_0: (○) PVF_2-1; (○) PVF_2-2; (□) PVF_2-3; (⊙) PVF_2-4; (△) PVF_2-5.

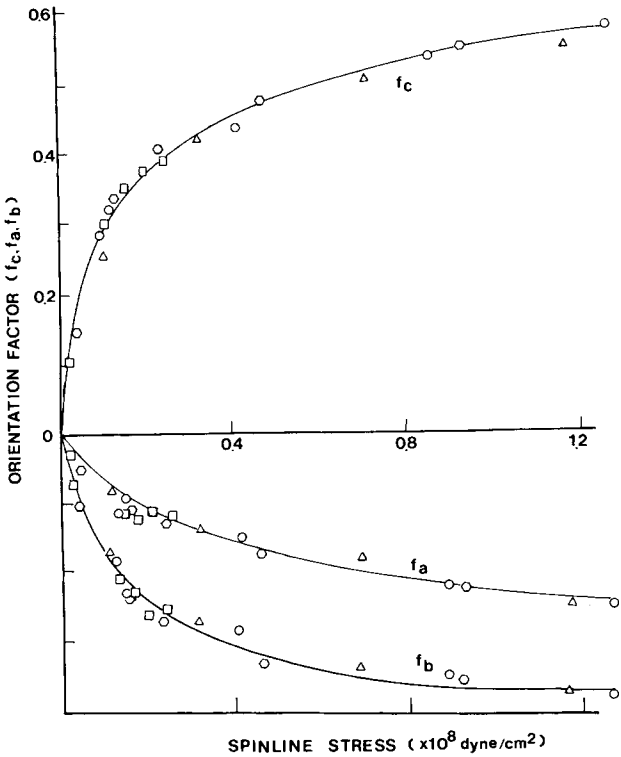

Fig. 9. Hermans–Stein orientation factors as a function of spinline stress for PVF_2 fibers: (○) PVF_2-1; (○) PVF_2-2; (□) PVF_2-3; (⊙) PVF_2-4; (△) PVF_2-5.

phases, f_c^α, f_c^β, and f_{am} are the Hermans or chain axis orientation factors of these three phases, and ϕ_α, ϕ_β, and ϕ_{am}, their volume fractions. The values of Δ_α^0, Δ_β^0, and Δ_{am}^0 seem not to be known for PVF_2.

In the melt prior to crystalline and in vitrified classes, the Hermans orientation factor is proportional to the spinline stress.[11] We have found f_c^α to be dependent upon stress and the relative quantities of ϕ_β and ϕ_α to be stress-dependent. This suggests that Δn should be a unique function of stress as in melt-spun fibers containing a single crystalline phase. (Compare Nadella et al.[11]) We plot Δn as a function of spinline stress in Figure 10. A good correlation is found.

Superstructure

The SALS pattern on the tapes may be interpreted in terms of changes in superstructure in the 0.1–4.0 μm range. The four-lobed H_v patterns with maxima off-zero angle indicate spherulitic structures, and the patterns with intensity maxima at zero angle have been previously described in the literature.[23,24] They represent spherulitic and oriented sheaf and rod structures, respectively. They have been previously noted in samples such as compression-molded and -cast polyethylene film. We seem to observe a similar transition here.

The transition from the typical spherulitic four-lobed patterns to sheaf-

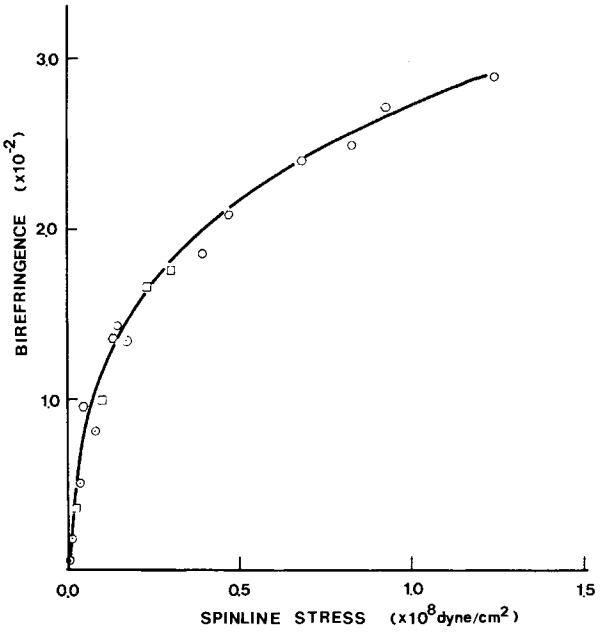

Fig. 10. Birefringence plotted as a function of spinline stress: (○) PVF_2-1; (○) PVF_2-2; (□) PVF_2-3; (⊙) PVF_2-4; (△) PVF_2-5.

and rodlike structure occurs first in PVF_2-1 followed by PVF_2-5 with increasing drawdown ratio. This suggests a transition at a critical stress. The high molecular weight PVF_2-1 shows a different rod structure from the intermediate molecular weight samples 5 and 2. PVF_2-1 shows contributions of spherulitic morphology only in quenched samples. Sample 4 only shows spherulitic patterns even at high drawdown ratios.

MECHANICAL PROPERTIES

Results

In Figure 11, we plot engineering stress $F(t)/A(0)$ as a function of strain $\Delta L/L_0$ for a series of melt spun PVF_2-2 fibers. We see that yield stress and tensile strength increase with V_L/V_0 while elongation to break decreases with increase of V_L/V_0. Similar trends are observed in the other materials.

Correlation with Spinning Conditions

The mechanical properties of the fibers are found to be correlatable with the spinning conditions. In Figures 12–14 we plot Young's modulus, tensile strength, and elongation to break as a function of spinline stress. Reasonably good correlations are obtained. Similar correlations have been obtained for polypropylene melt-spun fibers.[11,25]

Comparison to Other Polymers

We contrast the mechanical properties of PVF_2 fibers in Figure 15 with high density polyethylene. The moduli and tensile strength are generally higher at equivalent spinline stresses.

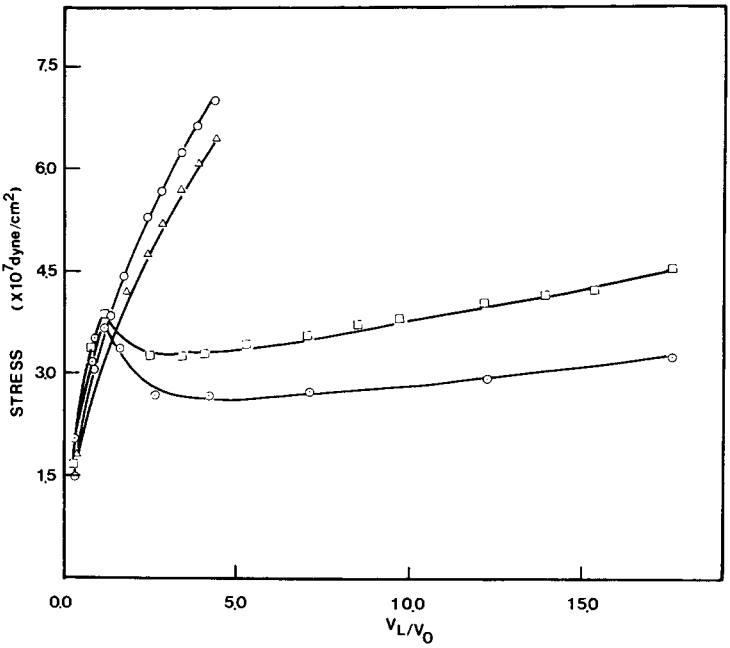

Fig. 11. Engineering stress–strain curves for PVF_2 fibers with $V_L/V_0 = 70$: (○) PVF_2-1; (□) PVF_2-2; (⊙) PVF_2-4; (△) PVF_2-5.

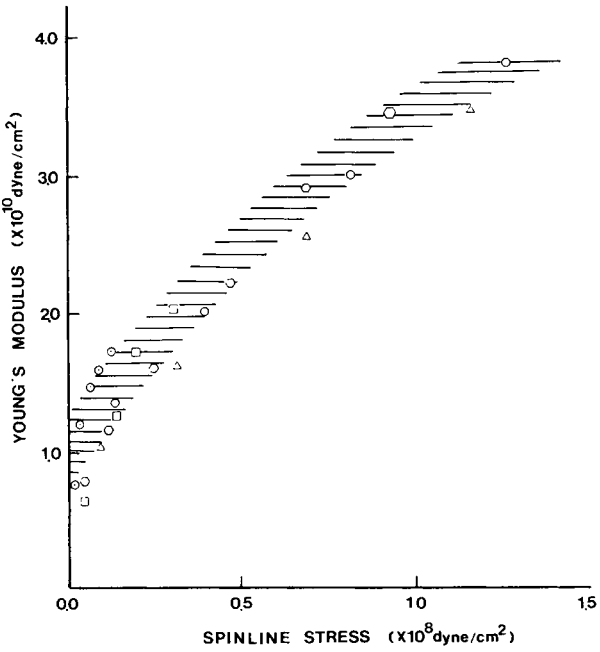

Fig. 12. Young's modulus as a function of spinline stress for melt spun PVF_2 fibers: (○) PVF_2-1; (○) PVF_2-2; (□) PVF_2-3; (⊙) PVF_2-4; (△) PVF_2-5.

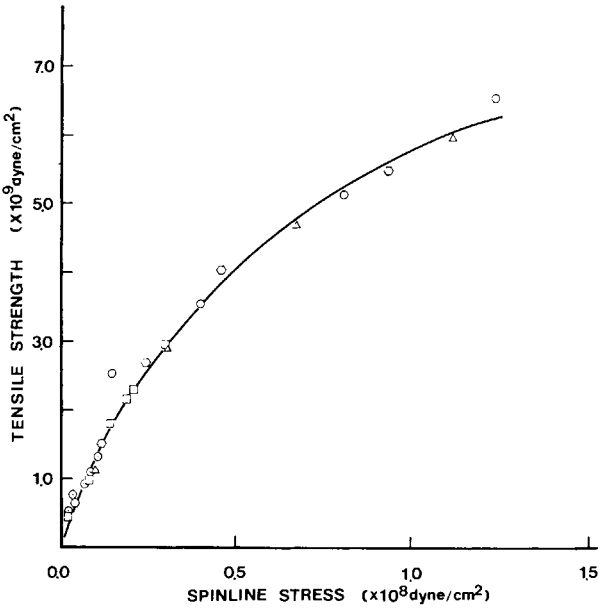

Fig. 13. Tensile strength as a function of spinline stress for melt spun PVF_2 fibers: (○) PVF_2-1; (○) PVF_2-2; (□) PVF_2-3; (⊙) PVF_2-4; (△) PVF_2-5.

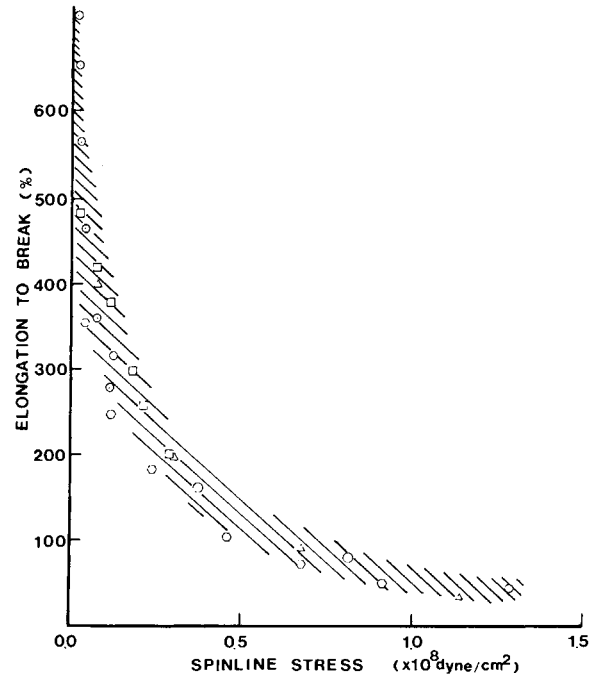

Fig. 14. Elongation to break as a function of spinline stress for melt spun PVF_2 fibers: (○) PVF_2-1; (○) PVF_2-2; (□) PVF_2-3; (⊙) PVF_2-4; (△) PVF_2-5.

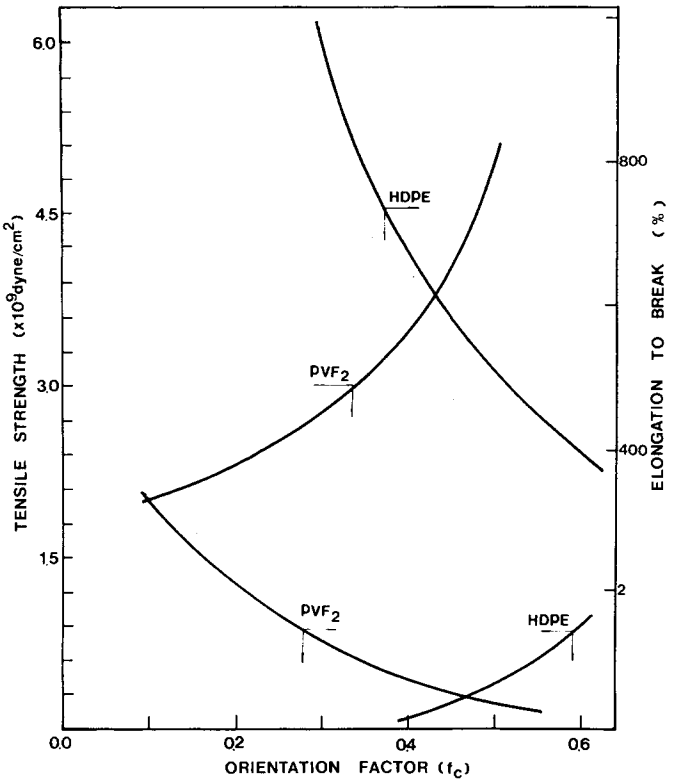

Fig. 15. Mechanical properties of melt spun PVF_2 compared with HDPEs.

CONCLUSIONS

1. Quiescently crystallized PVF_2 exhibits the α-crystalline form. Melt-spun PVF_2 fibers are polymorphic possessing both α and β crystalline forms, with the β phase first occurring at spinning stresses of 3×10^6 Pa. The β phase increases in quantity with increasing spinline stress. We believe that the β phase is derived by a stress-induced phase transition from the melt.

2. Crystalline orientation and mechanical properties in melt-spun fibers correlates with spinline stress independent of polymer molecular weight.

3. Tapes have been investigated by small angle light scattering. Four-lobed patterns indicating spherulitic structures are found in low viscosity materials and at low drawdowns in higher viscosity materials. Patterns suggesting rodlike structures are found at higher drawdowns in the higher molecular weight materials. The transition seems to be stress-dominated.

References

1. A. M. Glass, J. H. McFee, and J. G. Bergman, Jr., *J. Appl. Phys.*, **42**, 5219 (1971); J. H. McFee, J. G. Bergman, Jr., and G. R. Cram, *Ferroelectrics*, **3**, 305 (1972).
2. K. Nakamura and Y. Wada, *J. Polym. Sci., A-2*, **9**, 161 (1971).
3. J. B. Lando, H. G. Olf, and A. Peterlin, *J. Polym. Sci., A-1*, **4**, 941 (1966).
4. J. B. Lando and W. W. Doll, *J. Macromol. Sci. Phys.*, **B2**, 205 (1968).
5. W. W. Doll and J. B. Lando, *J. Macromol. Sci. Phys.*, **B2**, 219 (1968).
6. W. W. Doll and J. B. Lando, *J. Macromol. Sci. Phys.*, **B4**, 309 (1970).

7. R. Hasegawa, M. Kobayashi, and H. Tadokoro, *Polym. J.*, **3**, 591 (1972).
8. R. Hasegawa, Y. Takahashi, Y. Chatani, and H. Tadokoro, *Polym. J.*, **3**, 600 (1972).
9. M. Bachmann, W. L. Gordon, S. Weinhold, and J. B. Lando, *J. Appl. Phys.*, **51**, 5095 (1980).
10. S. Weinhold, M. H. Litt, and J. B. Lando, *Macromolecules*, **13**, 1178 (1980).
11. H. P. Nadella, H. M. Henson, J. E. Spruiell, and J. L. White, *J. Appl. Polym. Sci.*, **21**, 3003 (1977).
12. V. G. Bankar, J. E. Spruiell, and J. L. White, *J. Appl. Polym. Sci.*, **21**, 2341 (1977).
13. F. H. Muller, *Kolloid Z.*, **95**, 138 (1941).
14. R. J. Roe and W. R. Krigbaum, *J. Chem. Phys.*, **40**, 260B (1964).
15. P. H. Hermans and Platzek, *Kolloid Z.*, **88**, 68 (1939).
16. J. J. Hermans, P. H. Hermans, D. Vermaas, and A. Weidinger, *Rec. Trav. Chim.*, **65**, 427 (1946).
17. R. S. Stein, *J. Polym. Sci.*, **31**, 327 (1958).
18. K. Oda, J. L. White, and E. S. Clark, *Polym. Eng. Sci.*, **18**, 53 (1978).
19. T. Kitao, S. Ohya, J. Furukawa, and S. Yamashita, *J. Polym. Sci., A-2*, **11**, 1091 (1973).
20. J. R. Dees and J. E. Spruiell, *J. Appl. Polym. Sci.*, **18**, 1053 (1974).
21. P. H. Hermans, J. J. Hermans, D. Vermaas, and A. Weidinger, *J. Polym. Sci.*, **3**, 1 (1948).
22. R. S. Stein and F. H. Norris, *J. Polym. Sci.*, **21**, 381 (1956).
23. R. S. Stein and M. B. Rhodes, *J. Appl. Phys.*, **31**, 1873 (1960).
24. M. B. Rhodes and R. S. Stein, *J. Polym. Sci., A-2*, **7**, 1539 (1969).
25. H. P. Nadella, J. E. Spruiell, and J. L. White, *J. Appl. Polym. Sci.*, **22**, 3121 (1978).

Received October 2, 1984
Accepted October 23, 1984